

Numerical analysis of HRTF spectral characteristics based on sound pressures on a pinna surface

Makoto Otani (1), Yukio Iwaya (2), Yôiti Suzuki(2), and Kazunori Itoh (1)

(1) Faculty of Engineering, Shinshu University, 4-17-1 Wakasato, Nagano 380-8553, Japan

(2) Research Institute of Electrical Communication, Tohoku University, 2-1-1 Katahira, Aoba-ku, Sendai, 980-8577, Japan

PACS: 43.20.Fn, 43.66.Qp

ABSTRACT

Head-related transfer functions (HRTFs) play a crucial role in sound localization by human auditory system. Many researchers have investigated how HRTFs relate to sound localization, and have developed virtual auditory displays (VADs) which present virtual sound sources synthesized with HRTF-based audio signal processing. However, HRTFs have strong individuality because each listener's head and external ear shape differ. Therefore, an ideal 3D auditory space synthesis using HRTFs necessitates personal HRTF measurements or simulations, thereby degrading the versatility of such HRTF-based VADs. Resolution of problems related to HRTF individual variation necessitates clarification of a physical mechanism that yields spectral notches and peaks depending on a pinna shape. Researchers have therefore investigated the relation between HRTFs and the pinna shape using measurements of real and artificial heads or ear replicas. Moreover, numerical simulations, such as the boundary element method (BEM) or the finite difference time domain (FDTD) method, are considered as practical means to study this issue. As described herein, surface pressures on a pinna and HRTFs are calculated using BEM for various sound source elevation angles. The simulated surface pressures are analyzed in the time and frequency domains. Each boundary element on the surface is regarded as a secondary source radiating a sound wave corresponding to a reflection from the surface region, thereby enabling direct observation of a pinna's effects on HRTFs. Numerical results demonstrate the extent to which each part of a pinna contributes to a production of HRTF spectral notches and peaks depending on a source elevation.

INTRODUCTION

Human beings perceive a sound source's position; they localize a sound source by empirically using acoustical cues such as interaural time differences (ITDs), interaural level differences (ILDs) and spectral cues [1]. These cues are involved in head-related transfer functions (HRTFs) which represent acoustical transfer functions between a sound source and a listener's ears. A sound wave originating from a sound source reaches the ear with being affected by reflection, diffraction, and interference caused by a human body such as the head and pinna. Particularly, a pinna has a complicated structure that engenders a complex behavior of sound wave near an external ear and subsequently HRTFs' complex temporal and spectral characteristics depending on a source direction.

Many researchers have been studying the relation between HRTFs and pinna shape to clarify how the pinna affect HRTFs. Shaw and Teranishi performed an intensive investigation of this issue [2, 3], suggesting that various 'modes', or resonances, arise in an external ear and an ear canal; they produce peak and notch frequencies of HRTF spectra. Including these works in his overview, Blauert assessed related works and described that the pinna forms a system of acoustical resonators; the degree to which individual resonances of this system are excited depends on the direction and distance of the sound source. However, more precise investigations remain to be undertaken [1]. In addition to the frequency domain approach described above, a time-domain approach was also attempted to clarify pinna effects on HRTFs. Batteau described that echoes, actually *reflections*, from a pinna provide important cues for sound localization [4]. Furthermore, Yonezawa *et al.* observed echo patterns occurring in the pinna cavity using a pinna replica, enabling the

identification of pinna parts that provides first-order echoes [5].

Recently, numerical simulation has been presented as a practical means of predicting acoustic phenomena around the human head and external ears. HRTFs were numerically calculated based on a precise head model produced by an accurate 3D scanning device such as an optical scanner and a magnetic resonance imaging (MRI) device, *etc.* Various numerical methods were used such as the boundary element method (BEM) [6, 7, 8, 9, 10, 11, 12], the finite difference time domain (FDTD) method [13], and the finite element method (FEM) [14]. Not limited to providing an alternative mean to obtaining HRTFs rather than a real measurement, numerical simulation enables a systematic investigation of how the pinna shape performs as frequency-dependent and direction-dependent filter. Kahana *et al.* performed BEM simulation using a pinna model for numerical validation of the modes arising in concha measurements reported by Shaw *et al.*, showing that the numerical result agrees well with the measured one [15]. Takemoto *et al.* conducted FDTD simulation using a pinna model to investigate production mechanisms of spectral peaks and notches found in HRTFs [16]. These works examined a sound field around the external ear from the viewpoint of "resonance mode" arising in a pinna cavity.

The present work employs a different viewpoint and focuses on the sound pressures on pinna surface caused by the various source elevation, to investigate acoustic phenomena around the external ear and the pinna effects on HRTF spectral features. Kahana *et al.* also adopted such approach in their work [15], but he introduced the reciprocal theorem into the BEM simulation, in which a source and a receiver are interchanged. It can extremely reduce the computational time of HRTF calculations

for large number of sound source positions. However, an introduction of the reciprocal theorem hinders investigation of how the surface pressures vary with the source directions, because surface pressures can be calculated only for a source located at the ear-canal entrance. In this work, surface pressures on a pinna and HRTFs are numerically calculated for various sound source elevation angles. The simulated surface pressures are analyzed in the time and frequency domains. Each boundary element on the surface is regarded as a secondary source radiating a sound wave corresponding to a reflection from the surface region, thereby enabling direct observation of pinna effects on HRTFs.

BOUNDARY ELEMENT SIMULATION

This section presents an outline of the BEM used to simulate the acoustic phenomena related to HRTFs. The HRTF calculation with the BEM is categorized as an exterior problem that involves a scattering field around an object: the head in this case. The acoustic pressure $p(\mathbf{s})$ at position \mathbf{s} within the volume V can be written as

$$p(\mathbf{s}) = g_s \mathbf{A} - j\omega\rho \mathbf{G}_s \mathbf{V} - (\mathbf{G}_{ns} + j\omega\rho \mathbf{G}_s \mathbf{Y}) \hat{\mathbf{P}}, \quad (1)$$

where

$$g_s = [G(\mathbf{r}'_k|\mathbf{s})] \in \mathbf{C}^N,$$

$$\mathbf{G}_s = \left[\int \int_{S_j} G(\mathbf{r}_j|\mathbf{s}) dS \right] \in \mathbf{C}^M,$$

$$\mathbf{G}_{ns} = \left[\int \int_{S_j} \frac{\partial G(\mathbf{r}_j|\mathbf{s})}{\partial n} dS \right] \in \mathbf{C}^M,$$

$$\mathbf{A} = [q_1, q_2, q_3, \dots, q_N]^T \in \mathbf{C}^N,$$

$$\mathbf{V} = [v(\mathbf{r}_1), v(\mathbf{r}_2), v(\mathbf{r}_3), \dots, v(\mathbf{r}_M)]^T \in \mathbf{C}^M,$$

$$\mathbf{Y} = \text{diag}(y_n(\mathbf{r}_1), y_n(\mathbf{r}_2), y_n(\mathbf{r}_3), \dots, y_n(\mathbf{r}_M)) \in \mathbf{C}^{M \times M},$$

- M : the number of surface elements,
- N : the number of sources,
- S_j : the j -th surface element ($j = 1 \dots M$),
- \mathbf{r}'_k : point source position ($k = 1 \dots N$),
- \mathbf{r}_j : center of S_j ,
- p : acoustic pressure,
- G : the Green function,
- q_k : volume velocity of the source k ,
- ω : angular frequency,
- ρ : air density,
- n : normal vector,
- v : particle velocity in the normal direction,
- y_n : acoustic admittance in the normal direction.

Therein, $\hat{\mathbf{P}}$ is the acoustic pressures on the surface elements, *i.e.* surface pressures, given by solving the following equation:

$$\left(\frac{1}{2} \mathbf{I}_M + \mathbf{G}_n + j\omega\rho \mathbf{G}_s \mathbf{Y} \right) \mathbf{P} = g_s \mathbf{A} - j\omega\rho \mathbf{G}_s \mathbf{V}, \quad (2)$$

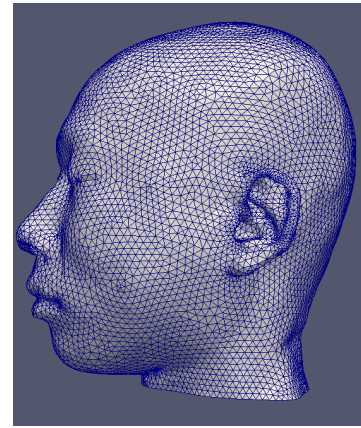
where

$$\mathbf{G}_n = \left[\int \int_{S_j} G(\mathbf{r}|\mathbf{r}_i) dS \right] \in \mathbf{C}^{M \times M},$$

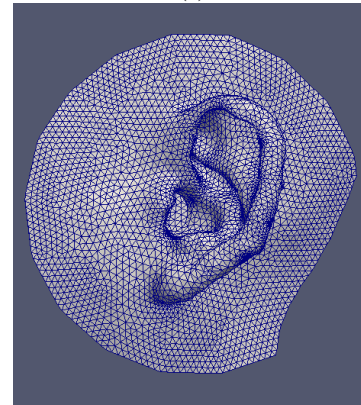
$$\mathbf{G} = \left[\int \int_{S_j} \frac{\partial G(\mathbf{r}|\mathbf{r}_i)}{\partial n} dS \right] \in \mathbf{C}^{M \times M},$$

$$g = [G(\mathbf{r}'_k|\mathbf{r}_i)] \in \mathbf{C}^{M \times N}.$$

Actually, $P(\mathbf{s})$ represents HRTF at a frequency of $\omega/(2\pi)$, if the receiver position \mathbf{s} is set at an entrance to the ear canal.



(a)



(b)

Figure 1: 3D shape models of (a) head and (b) external ear, which have 28,000 and 17,500 surface elements, respectively. The external ear shape model was discretized finer than the corresponding part of the head shape model.

Subsequently, head-related impulse responses (HRIRs) can be calculated by calculating $P(\mathbf{s})$ for all the required frequencies and by application of discrete Fourier transform (DFT) to them. The BEM for an exterior problem produces inaccurate solutions at eigenfrequencies of a corresponding interior problem, for which Eq. (1) has no unique solution. To resolve this so-called “non-uniqueness problem”, a combined Helmholtz integral equation formulation (CHIEF) method [17] is applied. In the CHIEF method, equations satisfying the condition that pressures at arbitrary points inside the boundary equal zero are added to the usual BEM formulation. The resulting over-determined linear system has a least-squares solution, enhancing the solution accuracy at eigenfrequencies of the corresponding interior problem.

COMPUTATIONAL MODEL

A head shape model and an external-ear model were constructed for application to the BEM simulation.

Head shape acquisition

A head and external ear shapes of one author were scanned using magnetic resonance imaging (MRI) scans (Magnex Eclips 1.5T; Shimadzu-Marconi) at ATR-BAIC. The scanning sequence was RF-FAST. The echo time (TE) was 4 ms, and the repetition time (TR) was 12 ms. Image size was 256×256 pixel; field of view (FOV), 256×256 mm; slice thickness, 1 mm; spatial resolution, $1.0 \times 1.0 \times 1.0$ mm. The subject lay face up in the MR imaging device. The MR images were recorded on a sagittal plane.

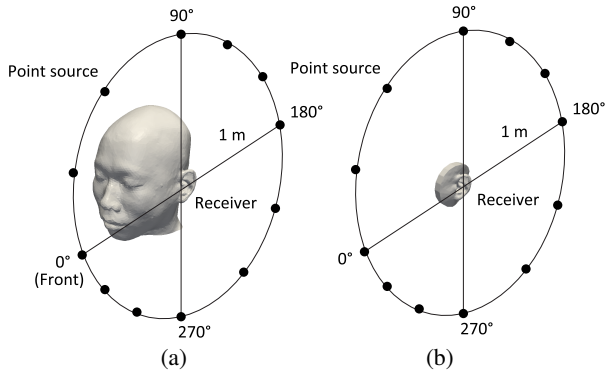


Figure 2: Source and receiver configurations for (a) head model and (b) external ear model. Point sources are located on a circle in the sagittal plane passing through the receiver, the entrance of the ear canal.

Head and external-ear shape models

A three-dimensional head shape model were constructed from MR scanned data using the following procedure. First, the MR images were edge-reinforced. Next, they were binarized based on the edge-reinforced sagittal, coronal, and horizontal images. Finally, a 3D head shape model was constructed by interpolation from the binarized volume data. Because the resulting head shape model has too large a number of surface elements to be calculated by the BEM with the current computational resources, it was remeshed to have approximately 28,000 surface elements, as presented in Fig. 1(a). An external-ear shape model was also developed by extracting the left external ear part, including its surrounding, from the original head shape model. This model was also remeshed to have a practical number of surface elements (17,500), as shown in Fig. 1(b). The ear canal of both models was modified to be in so-called blocked meatus condition [18], namely, it was filled solid at slightly inside from its entrance, which would eliminate the ear canal response from HRTFs. The external ear shape model has finer resolution in the surface discretization than the head shape model, which enables higher accuracy of the surface pressure. BEM simulation requires a fine surface discretization to produce accurate simulation results. As a rule of thumb, an edge length of each surface element should be smaller than, at least, 1/5 or 1/6 of target wavelength. The external ear shape model is valid up to 20 kHz with this criterion.

NUMERICAL CONDITION

Figures 2 (a) and (b) respectively depict the sources and receiver configuration for the head shape model and the external ear shape model.

Sound pressures on the surface elements and at a point adjacent to the entrance to left ear canal were calculated for ideal point sources. The sound sources were located 1 m distant from the receiver from 0 to 330° elevation angle at intervals of 30° in the sagittal plane passing through the receiver, not the head center. Here, 0° corresponds to the frontal position. The boundary condition of the model was set to be zero admittance, or infinite impedance, corresponding to the acoustically rigid surface. Calculated frequencies were from 86 Hz to 20 kHz at intervals of 86 Hz, which finally produce an impulse response of 512-pt length at a 44.1-kHz sampling rate.

In this work, HRTFs are not equalized: responses observed at the ear canal entrance are not divided by those observed at the head center without a head. However, non-equalized responses do not affect the results because the source distance is fixed at

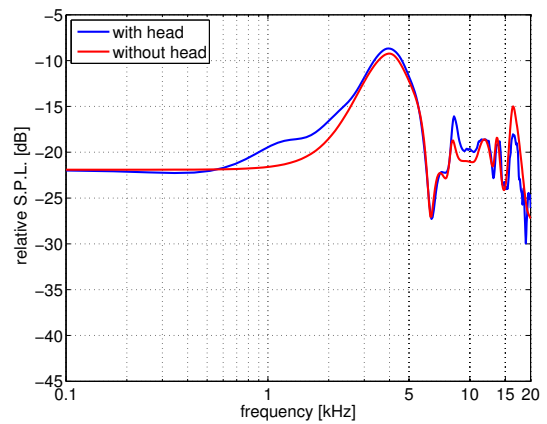


Figure 3: HRTFs at the left ear with and without the head. A sound source was located at the frontal position, *i.e.* 0° elevation angle. The ordinate and abscissa respectively represent relative sound pressure level in dB and frequency in kHz. Blue and red solid lines respectively represent corresponding results obtained with and without the head.

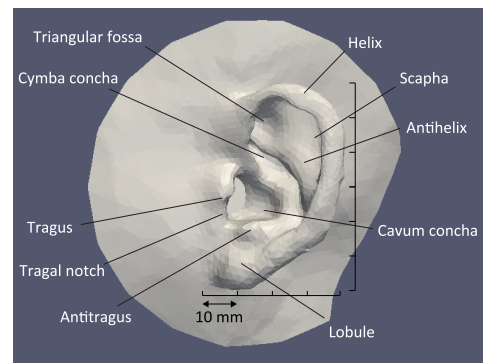


Figure 4: Name of pinna's parts.

1 m and the head-center response has flat frequency characteristics in the numerical simulation. Although such a definition of HRTFs differs from generally used one [1], impulse responses and their frequency characteristics observed at the ear canal entrance are referred to as HRIRs and HRTFs in this work.

Acoustical effects of the head

Although removal of the head from the computational model can ease the computational intensiveness, the lack of the head would affect the sound field around the external ear and subsequently the HRTFs. Figure 3 portrays HRTF amplitude spectra for a frontal sound source of 1-m distance by the head shape and the external ear shape models. A comparison of HRTFs between two models reveals some discrepancies between both results as shown in Fig. 3: the result obtained with the head has a broad spectral peak around 1 kHz which deviates from that without the head by as much as 4 dB; both results have different peak heights and notch depths at frequencies greater than 7 kHz by as much as 3 dB. However, fundamental spectral features are reproduced even with the external ear model, which indicates that the spectral peaks and notches appearing at higher frequencies are produced due to the pinna and its detail structures, although their heights and depths were affected by the head. Furthermore, because only sound sources in the sagittal plane are examined in this work, effects of the head would be

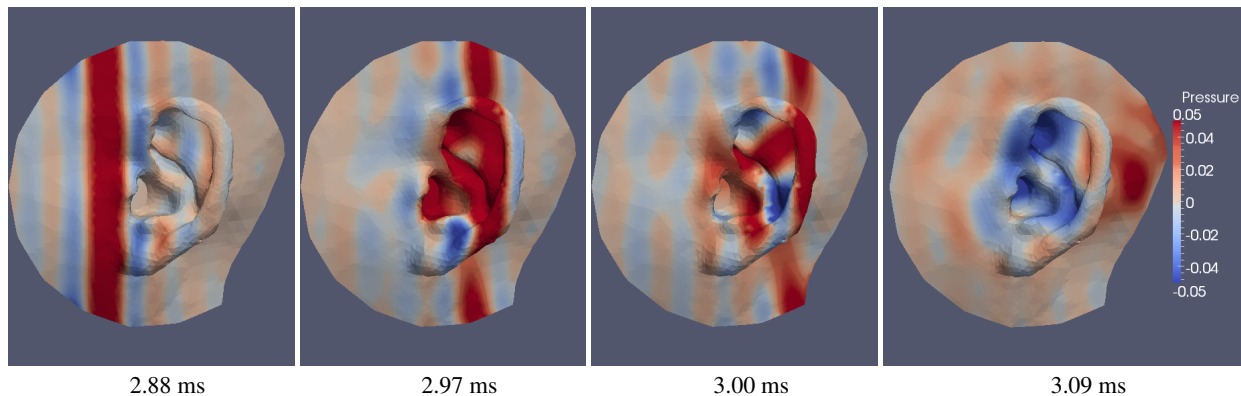


Figure 5: Pressure distribution on pinna surface in time domain (at 2.88, 2.97, 3.00, and 3.09 ms) for sound source located at 0° elevation angle.

smaller and less dependent on source position than those for sound sources in the horizontal plane. Therefore, the external ear shape model is used in BEM simulation hereafter, although the discrepancies between two models are of interest.

RESULTS

In this section, surface pressures on pinna are shown in both time and frequency domains based on the BEM simulation of the external ear shape model. Names of representative parts of the pinna are listed with external ear shape model in Fig. 4.

Time domain

Figure 5 presents an example of pressure distribution of the pinna surface and its surrounding parts. A point source is located in the frontal position, *i.e.* 0° elevation angle. Times are denoted below each panel as 2.88, 2.97, 3.00, and 3.09 ms. As the color bars demonstrate, colors represent the surface pressure's amplitudes where red and blue colors respectively indicate positive and negative values. In the color representation, the pressure values are clipped to emphasize smaller values arising on the pinna surface. The simulation was performed at a 44.1 kHz sampling rate.

The figure shows that the wavefront originating at the point source proceeds from 0° elevation angle. Surface elements behave as secondary sound sources having surface pressures as their strength. Sound waves radiated from secondary sound sources distributed on the surface correspond to reflections from the surface. At 2.88 ms, the larger positive pressures arising at the surface just in front of the pinna are excited mainly by a direct sound wave. When the direct sound wave reaches around the scapha (2.97 ms), the pinna surface including the concha and triangular fossae is most excited with positive pressure values. As the time proceeds (3.00 ms), although the direct sound wave almost passed the pinna, the pinna surface is excited with either positive or negative pressure depending on pinna parts. As the time proceeds further (3.09 ms) when the direct wave had entirely passed the pinna, the pinna surface is dominantly excited by negative pressures except for a lower part of the scapha. These results confirm that the pinna provides a sound-gathering effect and, subsequently, leads to a complicated pressure distribution pattern occurring in the pinna cavity depending on time.

Frequency domain

Figures 6 and 7 demonstrate pressure distributions on pinna surface in the frequency domain, *i.e.* steady-state responses, at 1.0, 4.3, and 5.7 kHz and at 8.6, 10.1, and 13.6 kHz, re-

spectively, where the HRTFs show remarkable characteristics. Sound sources are located at 60° , 180° , and 330° of elevation angle. The HRTF spectra for the corresponding source directions are also shown in the first row of the panel matrix with red solid lines representing free-field frequency characteristics, -22 dB flat, that would be observed at the receiver position. The free field responses were calculated using Green's function. The colors on the pinna surface represent relative sound pressure levels (SPLs) from -35 to -5 dB as shown by the color bars.

At 1.0 kHz where the HRTF amplitudes have almost same values among the three source elevations as shown in the first-row panels of Fig. 6, the pinna surface was homogeneously excited by around -22 dB irrespective of the source elevations.

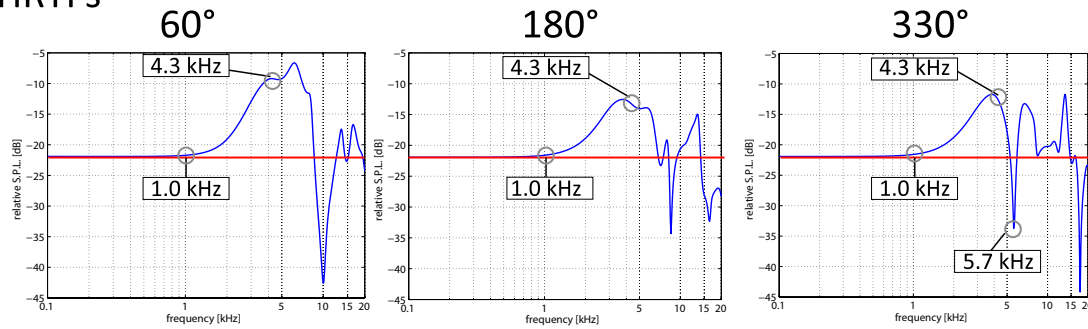
At 4.3 kHz where the HRTF spectra have broad peaks generally ranging from 2 to 5 kHz with direction-dependent variation in their maximum heights, the excited pinna parts differ depending on the source direction. For the 60° source elevation, SPL are large at the cavum and cymba conchae, the tragal notch, and the lower antihelix; for 180° , SPL are slightly smaller at the cavum and cymba conchae than 60° case, and are much smaller at other parts; for 330° , in addition to the cavum and cymba conchae, SPL are large as much as the conchae at the upper part of the pinna including the scapha, the antihelix, and the triangular fossa.

At 5.7 kHz, the HRTF spectrum has a deep spectral notch for 330° source elevation and, in contrast, it has spectral peaks for 60° and 180° source elevations. For 60° source elevation, SPL are uniformly large except at the upper part of cymba concha and the lower part of antihelix. For 180° source elevation, SPL are large at the cavum concha, the triangular fossa, and the scapha. For 330° source elevation, SPL are large except at the cavum concha. Only a source at 330° elevation produces low SPL at the cavum concha and a spectral notch in HRTF at this frequency, although sources at other elevations produce high SPL at the cavum concha and no spectral notch in HRTFs.

At 8.6 kHz where the HRTF has a spectral notch for 180° source elevation, and not for other source elevations, SPL is prominently smaller at the cavum concha for 180° case than other cases. In addition, at 10.1 kHz, where the HRTF has a spectral notch for 60° source elevation, SPL is smaller at the cavum concha for 60° case than other cases.

At 13.6 kHz, where spectral peaks appear in HRTFs for all the source elevations, the surface pressure distributions become more complicated. However, those in the cavum concha are mutually similar. This common distribution pattern is explainable by a resonance "mode" arising in the cavum concha cavity

HRTFs



Surface pressures

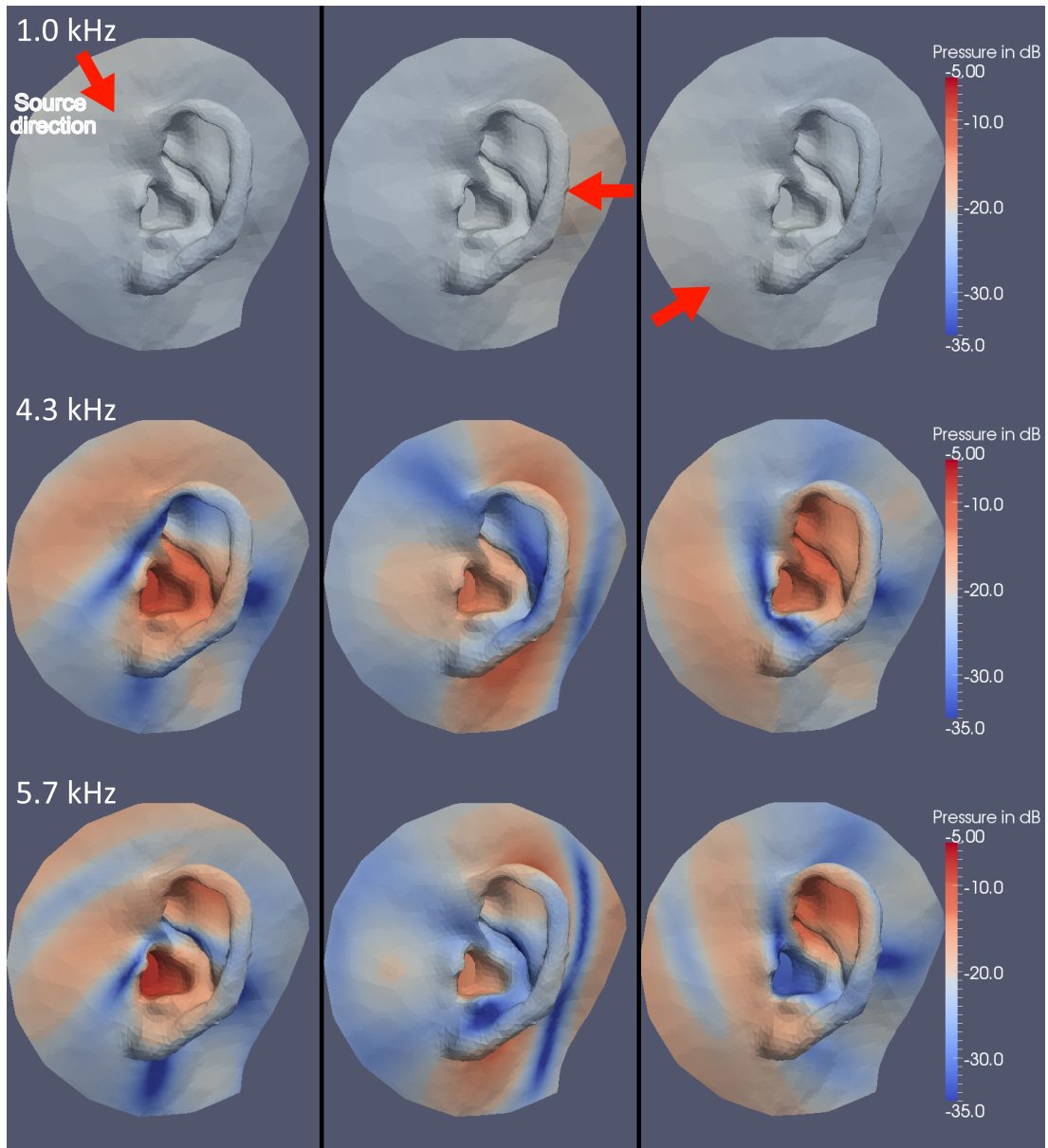


Figure 6: Pressure distributions on the pinna surface in frequency domain in 3×3 matrix format whose column corresponds to sound source elevations of 60, 180, and 330° and whose rows corresponds to frequencies of 1.0, 4.3, and 5.7 kHz. The HRTF spectra for the corresponding source angles are also shown in the first row with red solid lines representing free-field frequency characteristics that would be observed at the receiver position (-22 dB flat). Red arrows indicate the directions from which the sound waves come. The color bars indicate relative sound pressure levels ranging from -35 to -5 dB.

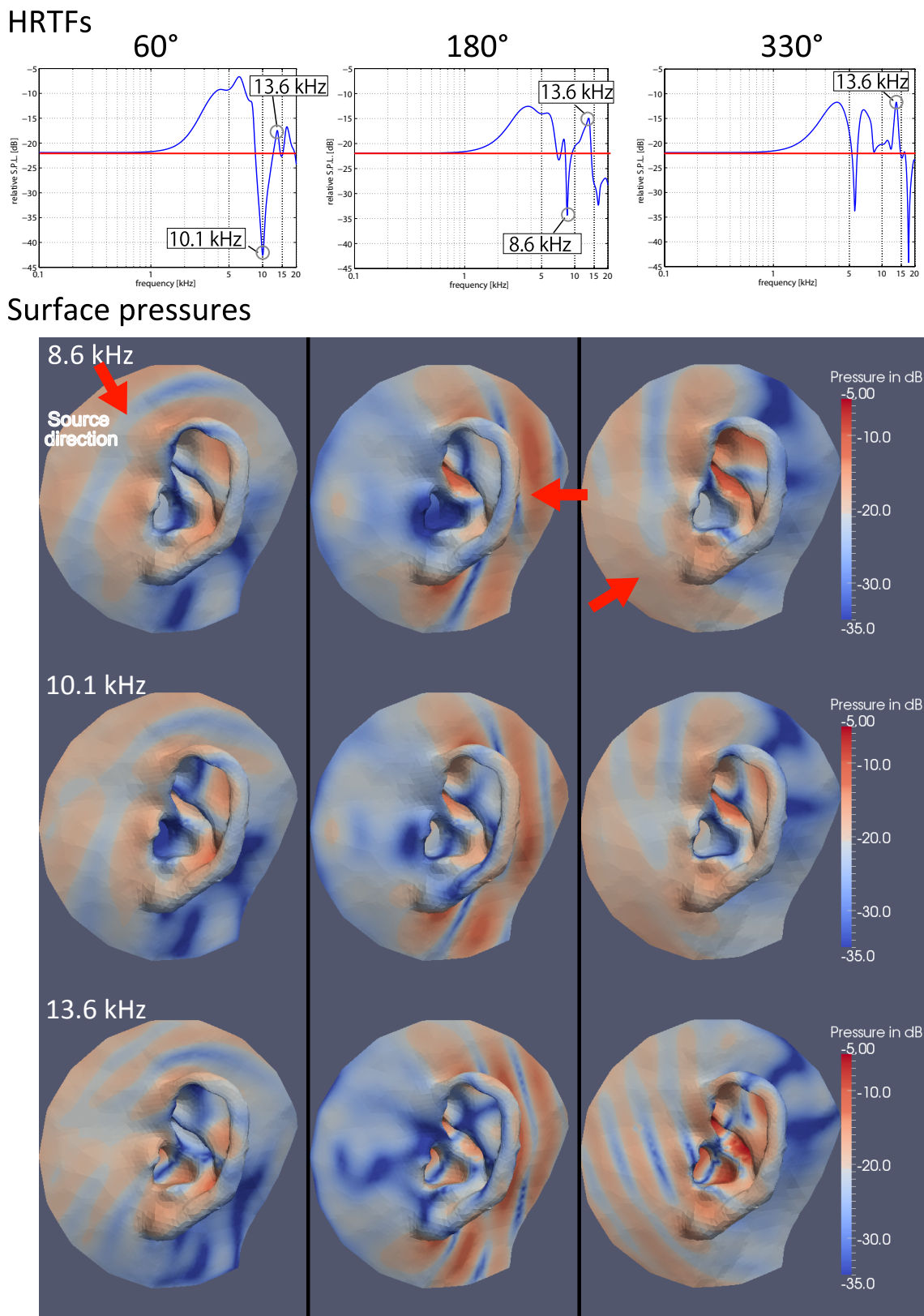


Figure 7: Pressure distributions on pinna surface in the frequency domain at higher frequencies, 8.6, 10.1, and 13.6 kHz. Details of figure format are the same as those shown in Fig. 6.

having very small SPLs along a vertical “nodal line” and large SPL on other surface of the cavity, which could yield the spectral peaks at this frequency irrespective of the source elevation. However, the “mode” shape varies slightly with the source elevation, which indicates that such variation in the “mode” shape depending on the source elevation produced the variation in height of the spectral peaks among the different source elevations.

DISCUSSIONS

In addition, from the time-domain analysis, a pinna’s sound-gathering effects are visible in the results for 4.3 and 5.7 kHz. For 0° source elevation, the pinna surface is entirely excited more or less depending on the frequency. For 330° source elevation, namely when the source is located slightly lower than the frontal position, the upper parts of the pinna, such as the scapha and the triangular fossa, are especially excited irrespective of the frequency, which indicates that a sound wave from below is “captured” by the upper parts of pinna. For 180° source elevation, *i.e.* rear position, the entire pinna surface is not prominently excited compared with other source elevations, showing that a sound wave from rear reaches to the pinna surface after being attenuated by scattering at a pinna’s back surface.

At 4.3 kHz, although the upper parts of pinna are more excited for source elevation of 330° than 180°, no prominent difference exists in the heights of spectral peaks at 4.3 kHz between both source elevations, which indicates that the effects of the cavum and cymba conchae are greater than those of other parts. At 5.7 kHz for 330° source elevation, although the upper parts of pinna are excited as much as at 4.3 kHz, the HRTF for 330° source elevation has a spectral notch at 5.7 kHz. This difference can be attributed to the very low surface pressures at the cavum concha, which indicates the dominant effects of the cavum concha at this frequency. At higher frequencies, spectral features examined in this work seem to depend mainly on the surface pressures at the cavum concha that is the closest part to the receiver, *i.e.* the ear-canal entrance. Considering the relevance between a wavelength and a distance from the receiver to a reflecting “wall”, it is reasonable that pinna parts closer to the ear-canal entrance affect the HRTFs more dominantly as the frequency increases.

Shaw reported that, from the average characteristics for 10 subjects, six modes occur under blocked meatus condition in a pinna cavity at 4.2, 7.1, 9.6, 12.1, 14.4, and 16.7 kHz [19]. These resonance frequencies and their mode shapes are expected to vary among subjects. However, the results at 4.3 and 13.6 kHz in the current work are comparable to the modes at 4.2 and 14.4 kHz, respectively, in the results by Shaw. In the literature, it is reported that the mode at 4.2 kHz occurs omnidirectionally irrespective of the source direction. This omnidirectional feature of this mode can be found in the current work. In addition, according to Shaw’s work, it is demonstrated that the mode at 14.4 kHz has two “nodal lines” in the cavum and cymba conchae cavity: one runs vertically along a median line of the cavum and cymba conchae; another runs horizontally along the boundary of the cavum and cymba conchae. Such a mode shape is also observed at 13.6 kHz in the current work. The comparisons between the modes and the surface pressures described above indicate that a certain relevance exists between the “mode” in the pinna cavity, especially the concha cavity, and the surface pressures on the pinna. However, the results in the current work reveal that pinna surface pressures have various distribution patterns greatly depending on source elevations. As described in [1], a source direction affects the degree to which each mode is “excited”. The results in this work show that “mode” shape as well as “mode amplitude” varies with source elevations.

CONCLUSION

As described in this paper, surface pressures on the pinna, as well as HRTFs, are numerically simulated by the BEM and the external ear shape model constructed using a MRI scanning device. Subsequently, relation between representative spectral peaks and notches and surface pressures are discussed.

Results of the time-domain analysis of the surface pressures demonstrates that a pinna provides sound-gathering effects. Such effects, subsequently, leads to a complicated pressure distribution pattern on a pinna surface which varies greatly depending on time. Moreover, the frequency-domain analysis reveals that surface pressure distribution on the pinna relates to a production of spectral peaks and notches in HRTFs. The results show that pinna parts closer to the ear canal entrance provide more dominant effects on the HRTFs as the frequency increases. The “modes” arising in the pinna cavity reported in the literature [19] are also confirmed in this work, showing that the degree to which the each mode is excited depends on the source direction. In addition, the pressure distribution pattern, which corresponds to “mode shape”, also depends on source directions, which yield HRTF directional characteristics.

ACKNOWLEDGMENT

This research was supported in part by Grant-in-Aid for Young Scientists (B) (No. 21700128) and Grant-in-Aid for Specially Promoted Research (No. 19001004) of The Ministry of Education, Culture, Sports, Science and Technology (MEXT), Japan.

REFERENCES

- [1] J. Blauert, *Spatial Hearing*, revised ed. (The MIT press, Cambridge, 1997).
- [2] E.A.G. Shaw and R. Teranishi, “Sound pressure generated in an external-ear replica and real human ears by a nearby point source,” *J. Acoust. Soc. Am.* **44**(1), 240–249 (1967).
- [3] R. Teranishi and E.A.G. Shaw, “External-ear acoustic models with simple geometry,” *J. Acoust. Soc. Am.* **44**(1), 257–263 (1967).
- [4] D.W. Batteau, “The role of the pinna in human localization,” *Proc. R. Soc. London, Ser. B168* 158–180 (1967).
- [5] Y. Yonezawa and K. Itoh, “Characteristics of pulse sound reflection and scattering on the external ear,” *IEICE Trans. on Fundamental* **J70-A**(8), 1186–1194 (1987).
- [6] B.F.G. Katz, “Boundary element method calculation of individual head-related transfer function. I. Rigid model calculation,” *J. Acoust. Soc. Am.* **110**(5), 2440–2448 (2001).
- [7] Y. Kahana, P.A. Nelson, M. Petyt and S. Choi, “Boundary element simulation of HRTFs and sound fields produced by virtual acoustic imaging systems, Proc. 105th AES Convention, No. 4817 (1998).
- [8] T. Walsh, L. Demkowicz, and R. Charles, “Boundary element modeling of the external human auditory system,” *J. Acoust. Soc. Am.* **115**(3), 1033–1043 (2004).
- [9] S. Takane, T. Matsushashi, and T. Sone, “Numerical estimation of individual HRTFs by using BEM,” *Proc. International Congress on Acoustics* (2004).
- [10] M. Otani and S. Ise, “Fast calculation system specialized for head-related transfer function based on boundary element method,” *J. Acoust. Soc. Am.* **119**(5), 2589–2598 (2006).
- [11] M. Otani, T. Hirahara, and S. Ise, “Numerical study on source distance dependency of head-related transfer functions,” *J. Acoust. Soc. Am.* **125**(5), 3253–3261 (2009).

- [12] Y. Iwaya and Y. Suzuki, “Numerical analysis of the effects of pinna shape and position on the characteristics of head-related transfer functions,” *Proc. of Forum Acusticum 2008* (2008).
- [13] P. Mokhtari, H. Takemoto, R. Nishimura, and H. Kato, “Comparison of simulated and measured HRTFs: FDTD simulation using MRI head data,” *Audio Engineering Society 123rd Convention Paper 7240*, New York, NY, USA (2007).
- [14] H. Muraoka, Y. Takahashi, T. Haedar, M. Otani, and T. Hirahara, “The head related transfer function simulation by FEM/IEM and reciprocal theorem,” *Proc. of 19th International Congress on Sound and Vibration*, CD-ROM, Cairns (2007).
- [15] Y. Kahana and P.A. Nelson, “Numerical modelling of the spatial acoustic response of the human pinna,” *J. Sound & Vib.* **292** 148–178, (2006).
- [16] H. Takemoto, P. Mokhtari, H. Kato, and R. Nishimura, “Pressure distribution patterns on the pinna at spectral peak and notch frequencies of head-related transfer functions in the median plane,” *Proc. of International Workshop on the Principles and Applications of Spatial Hearing I-11*, Zao (2009).
- [17] H.A. Schenck, “Improved integral formulation for acoustic radiation problems,” *J. Acoust. Soc. Am.* **44**, 41–58 (1968).
- [18] H. Møller, “Fundamentals of binaural technology,” *Appl. Acoust.* **36**, 171–218 (1992).
- [19] E.A.G. Shaw, “Acoustical features of the human external ear,” in R.H. Gilkey, T.R. Anderson (Eds.), *Binaural and Spatial Hearing in Real and Virtual Environments*, (Lawrence Erlbaum Associates, Mahwah, NJ, 1997).